Hydrogen storage properties of Mg-based composites prepared by reaction ball milling

2006 J. Phys.: Condens. Matter 18 11275

(http://iopscience.iop.org/0953-8984/18/49/019)

INSTITUTE OF PHYSICS PUBLISHING JOURNAL OF PHYSICS: CONDENSED MATTER

J. Phys.: Condens. Matter **18** (2006) 11275–11290 doi:10.1088/0953-8984/18/49/019

Hydrogen storage properties of Mg-based composites prepared by reaction ball milling

M Kandavel and S Ramaprabhu[1]

Alternative Energy Technology Laboratory, Department of Physics, Indian Institute of Technology Madras, Chennai-600 036, India

E-mail: ramp@iitm.ac.in

Received 23 February 2006, in final form 18 September 2006
Published 22 November 2006
Online at stacks.iop.org/JPhysCM/18/11275

Abstract

The effect of amount of AB_2 alloy on the hydrogen storage properties of Mg-based composites is investigated. Mg + x wt% $Ti_{0.1}Zr_{0.9}Mn_{0.9}V_{0.1}Fe_{0.5}Ni_{0.5}$ (x = 5, 15, 25, 30, 35, 40, 50, 60 and 75) composites have been prepared by reaction ball milling Mg with $Ti_{0.1}Zr_{0.9}Mn_{0.9}V_{0.1}Fe_{0.5}Ni_{0.5}$ and characterized by powder x-ray diffractograms and scanning electron microscopy. Pressure–composition absorption isotherms of these composites have been obtained in the pressure range 0.1–30 bar at 300 °C using the pressure reduction technique. Maximum storage capacity of around 4.8 wt% at 300 °C has been achieved in Mg + 5 wt% $Ti_{0.1}Zr_{0.9}Mn_{0.9}V_{0.1}Fe_{0.5}Ni_{0.5}$. The dependence of hydrogen absorption plateau pressure on the unit cell volume of Mg phase in these composite materials is discussed. Thermal desorption of hydrogen has been studied using differential scanning calorimetry. Hydrogen absorption/desorption kinetics of these composites have been performed at 300 °C, and for Mg + 25 wt% $Ti_{0.1}Zr_{0.9}Mn_{0.9}V_{0.1}Fe_{0.5}Ni_{0.5}$ kinetics of absorption have been performed in the temperature range 250–325 °C. The absorption kinetics data have been analysed using rate equations to understand the mechanism of the hydriding reaction process and to obtain the activation energy.

1. Introduction

Metal hydrides have been the focus of recent intensive research activities on hydrogen storage. Among the different types of metal hydrides, magnesium and Mg-based systems are recognized as the most promising material for hydrogen storage because of their high hydrogen storage capacity and because they are inexpensive [1]. However, slow reaction kinetics, high dissociation temperature and a hard activation process are the main drawbacks of the Mg-based systems. Moreover, Mg usually needs to be activated by being exposed to a high

[1] Author to whom any correspondence should be addressed.

temperature and high hydrogen pressure for longer time. This is due to the formation of a magnesium oxide layer over the Mg matrix, which is impermeable to hydrogen. Recently many researchers have studied the hydrogen storage properties of Mg-based composites using certain catalysts such as metals, alloys and oxides to improve the sorption kinetics and activation process [2–5]. Hydrogen absorption properties of Mg-based systems have been improved by many approaches, mainly by (a) addition of alloying elements, (b) formation of composite materials with different catalysts such as metals, alloys, intermetallics and oxides and (c) surface modification of Mg by fluoride treatment, nanocrystalline/amorphous microstructures [6–8]. Hydrogen storage properties of a composite material mainly depend on the interaction between the different components present in the system. The hydriding properties of the poor kinetic component (Mg) can be catalytically improved by the addition of a good kinetic component (catalyst). Zuluska *et al* [9] have improved the hydrogen storage properties of MgH_2 by producing a nanocrystalline form using ball milling and by adding nanoparticles of Pd over the surface of Mg. Hu *et al* [10] showed the uniform distribution of alloy particles over an Mg matrix in Mg + 30 wt% $TiMn_{1.5}$ composite material and thereby an increase in sorption kinetics. Recently, reaction ball milling (RBM) has been introduced for the preparation of hydrogen storage materials. Hydrogen absorption studies on non-stoichiometric Zr based alloys [11] revealed that $Ti_{0.1}Zr_{0.9}Mn_{0.9}V_{0.1}Fe_{0.5}Ni_{0.5}$ has fast hydrogen absorption kinetics at room temperature. In the present paper, the results obtained from the pressure–composition (P–C) isotherms at 300 °C, thermal desorption and kinetics of absorption/desorption studies of Mg + x wt% $Ti_{0.1}Zr_{0.9}Mn_{0.9}V_{0.1}Fe_{0.5}Ni_{0.5}$ (x = 5, 15, 25, 30, 35, 40, 50, 60 and 75) composites have been discussed. In addition, the absorption isotherms of Mg + 25 wt% $Ti_{0.1}Zr_{0.9}Mn_{0.9}V_{0.1}Fe_{0.5}Ni_{0.5}$ composite in the range 200–350 °C and the desorption isotherm at 300 °C have been performed in order to find the hysteresis.

2. Experimental details

$Ti_{0.1}Zr_{0.9}Mn_{0.9}V_{0.1}Fe_{0.5}Ni_{0.5}$ has been prepared in an arc furnace under an argon atmosphere of about 0.80 bar with stoichiometric proportions of high-purity constituent elements as mentioned in [11]. Mg + x wt% $Ti_{0.1}Zr_{0.9}Mn_{0.9}V_{0.1}Fe_{0.5}Ni_{0.5}$ (x = 5, 15, 25, 30, 35, 40, 50, 60 and 75) composite materials have been prepared by reaction ball milling Mg and alloy powder in a tungsten carbide bowl under hydrogen atmosphere in a P5 ball mill for 10 h. The ball to powder ratio (BPR) was kept to 10:1. Hydrogen gas was introduced into the bowl every hour again to keep the hydrogen atmosphere at ∼1 bar. The composite materials were then characterized by powder x-ray diffractograms (XRD) and scanning electron microscopy (SEM). The P–C absorption isotherms of these composite materials at 300 °C in the pressure range 0.1–30 bar were obtained using a conventional gasometric technique. The system was calibrated at various initial pressures and the sample cell volume has been measured with van der Waals correction for the volume of the gas molecules and molecular interactions. Several blank tests were carried out at different initial pressures and the drop in pressure during the same time interval as that of the experiment was taken into account while calculating the sample cell volume, and hence for the precise measurement of the hydrogen adsorption capacity extreme care was taken to eliminate the leakage of the system [12]. About 0.5 g of sample in the form of a pellet was introduced in the high-pressure reactor and evacuated to 10^{-6} Torr. For activation purposes, composite powders were exposed to hydrogen atmosphere at a pressure of 20 bar and a temperature of 300 °C. From the reduction of hydrogen pressure, the amount of hydrogen absorbed by the composite material has been calculated. As in a high-pressure experiment the pressure changes arising from temperature variations can be mistakenly interpreted as substantial absorption, the room temperature in our laboratory was maintained at 25 ± 1 °C.

All these effects including the inherent leakage of the system were taken into account in the analysis of the hydrogen absorption results as suggested in [11]. The P–C relationships were obtained by calculating the hydrogen storage capacity in wt% from the pressure drop during the hydrogen absorption at constant temperature. Dehydriding was performed by evacuating and heating the hydride powder at 400 °C for 3 h. After three such absorption/desorption cycles, the amount of hydrogen absorbed by the composite remains the same. After the activation process, absorption/desorption isotherm data were collected; following each experiment, the sample was degassed at 400 °C under a vacuum of 10^{-6} Torr. After P–C isotherm measurements, hydride powders were collected for thermal desorption studies using differential scanning calorimetry (DSC, Netzsch DSC 200 PC). DSC studies have been carried out for these composite hydrides at a heating rate of 10 °C min^{-1} under argon atmosphere. The kinetics data were collected by recording the change in pressure as a function of time at constant temperature. The accuracy in the temperature measurement is ±1 °C.

3. Results and discussion

3.1. Structural studies

$Ti_{0.1}Zr_{0.9}Mn_{0.9}V_{0.1}Fe_{0.5}Ni_{0.5}$ alloy crystallizes in C14 Laves phase hexagonal structure with a space group $P6_3/mmc$ and structural details are given elsewhere [11]. Figures 1 and 2 show the room temperature Cu Kα powder XRD patterns of 10 h reaction ball milled Mg+x wt% $Ti_{0.1}Zr_{0.9}Mn_{0.9}V_{0.1}Fe_{0.5}Ni_{0.5}$ (x = 5, 15, 25, 30, 35, 40, 50, 60 and 75) composites. The XRD patterns show the existence of Bragg reflections corresponding to Mg and alloy particles. In addition, Bragg reflections corresponding to MgH_2 are also observed in these composites, and after x = 35 wt%Mg_6Ni secondary phase formation is observed. In gas–solid reaction, the formation of MgH_2 requires a very high pressure and high temperature. The formation of MgH_2 at room temperature and at low hydrogen pressure during reaction milling under hydrogen atmosphere can be explained by the exposure of fresh surface of Mg and alloy particles continuously to the hydrogen atmosphere, dispersion of $Ti_{0.1}Zr_{0.9}Mn_{0.9}V_{0.1}Fe_{0.5}Ni_{0.5}$ alloy particles on the surface of Mg matrix, dissociation of hydrogen molecules into atoms due to catalytic $Ti_{0.1}Zr_{0.9}Mn_{0.9}V_{0.1}Fe_{0.5}Ni_{0.5}$ alloy particles and the decrease in grain size of Mg due to the increase in milling time. Since the changes in the lattice parameters were very small, the lattice parameters have been more precisely obtained by using Si as the standard by mixing Si with these composite materials while taking the diffractograms. The intensity of reflections corresponding to $Ti_{0.1}Zr_{0.9}Mn_{0.9}V_{0.1}Fe_{0.5}Ni_{0.5}$ increases with the increase of alloy content. The lattice parameters and unit cell volumes of Mg (hexagonal $P6_3/mmc$) and alloy (hexagonal $P6_3/mmc$) phases have been separately evaluated using a least square refinement technique and are listed in table 1. Figure 3(a) shows the variation of unit cell volumes of Mg and AB_2 alloy phases with the amount of catalyst (x). The unit cell volumes of Mg and alloy phases increase with alloy content up to about 35 wt% and then decrease. The initial increase in the unit cell volumes of Mg and AB_2 phases increase due to the hydrogenation of these two phases during reaction ball milling. Zr-based AB_2 type alloys are known to undergo a large volume expansion (around 25%) in the β-phase. Recent XRD studies of AB_2 alloy hydrides show a volume expansion of around 1.9 $Å^3$ in the α phase [13]. Further, hydrogen storage properties of nanostructured Mg catalysed with various elements show that the unit cell volume of Mg increases with hydrogen concentration [14]. In order to confirm the effect of hydrogen in the initial increase in the unit cell volume of Mg and AB_2 phases, we have prepared the composites under argon atmosphere instead of hydrogen atmosphere. XRD patterns of Mg-based composites prepared under argon atmosphere show the existence of Mg and AB_2 Bragg

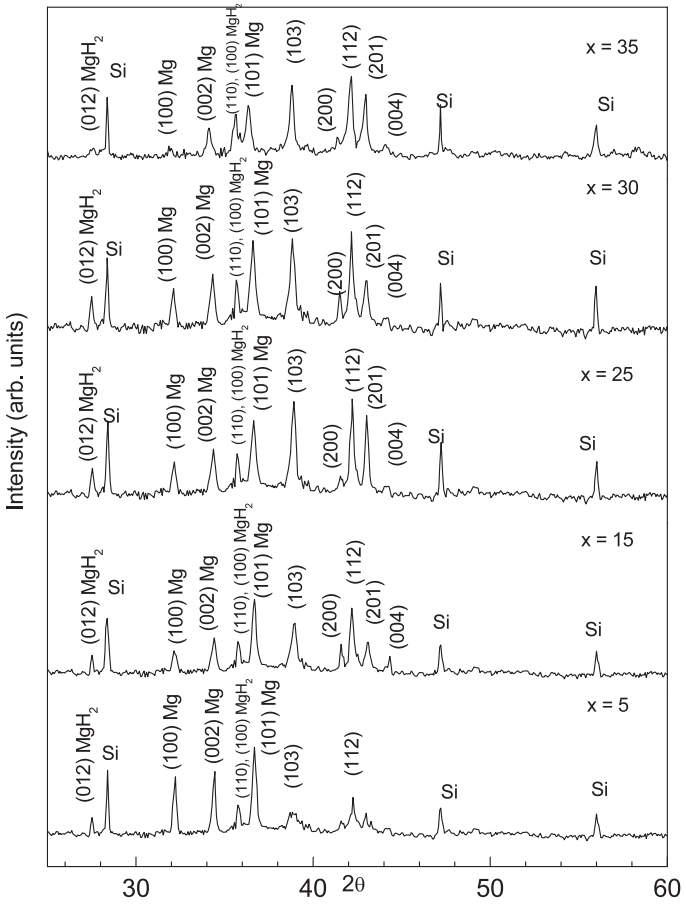

Figure 1. XRD patterns of Mg + x wt% $Ti_{0.1}Zr_{0.9}Mn_{0.9}V_{0.1}Fe_{0.5}Ni_{0.5}$ (x = 5, 15, 25, 30 and 35) composite materials.

reflections and there is no Mg_6Ni secondary phase formation. The unit cell volumes of Mg and AB_2 phases of Mg-based composites prepared under argon atmosphere show that there is no variation in the unit cell volume (figure 3(b)). This implies that the initial increase in the unit cell volume of Mg and AB_2 phases is due to hydrogen absorption by these phases during reaction ball milling.

After $x = 35$ wt%, unit cell volumes of these two phases decrease with increase in the AB_2 concentration. The decrease in unit cell volume of AB_2 phase after $x = 35$ wt% is due to the formation of Mg_6Ni secondary phase as revealed from the powder XRD patterns (figures 1 and 2). The formation of Mg_6Ni phase indicates that Ni is separated out from the alloy and it combines with Mg to form Mg_6Ni, which leads to lattice contraction of AB_2 phase. Decrease in the unit cell volume of Mg phase after $x = 35$ wt% is due to the formation of Mg solid solution with any of the elements present in $Ti_{0.1}Zr_{0.9}Mn_{0.9}V_{0.1}Fe_{0.5}Ni_{0.5}$. Previous literature shows that Ni and Fe will not form a solid solution with Mg due to the large size mismatch [15]. Ti, Zr, Mn and V are the possible elements which can form a solid solution with Mg [16, 17]. However, the solid solubility of Mn and V in Mg is very small. If Zr forms a solid solution with Mg, there will not be any change in lattice volume because the atomic radii of Mg and Zr are almost equal. So the decrease in the unit cell volume of

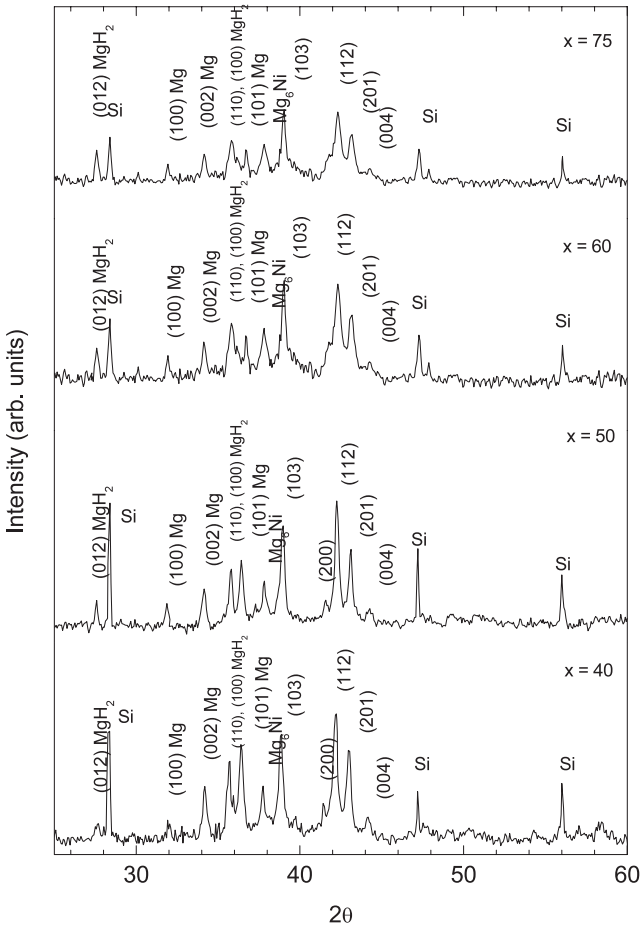

Figure 2. XRD patterns of Mg + x wt% $Ti_{0.1}Zr_{0.9}Mn_{0.9}V_{0.1}Fe_{0.5}Ni_{0.5}$ (x = 40, 50, 60 and 75) composite materials.

Mg phase can be explained due to the formation of Mg–Ti solid solution. Further, the solid solubility of Ti in Mg is very high, around 12% [17]. In order to confirm the above explanation, we have prepared AB_2 alloys without Ti content ($ZrMn_{0.9}V_{0.1}Fe_{0.5}Ni_{0.5}$) and synthesized Mg + x wt% $ZrMn_{0.9}V_{0.1}Fe_{0.5}Ni_{0.5}$ composites by milling under hydrogen atmosphere. XRD patterns of these composites (prepared using the alloy without Ti) confirmed the presence of Mg, AB_2, MgH_2 and Mg_6Ni phases. Variation of unit cell volume of Mg and AB_2 phases with alloy concentration is shown in figure 3(c). The unit cell volume of Mg phase increases even after $x = 35$ wt%. This implies that the Mg does not form solid solution with any of the elements present in the alloy. Thus the decrease in the unit cell volume of Mg phase in Mg + x wt% $Ti_{0.1}Zr_{0.9}Mn_{0.9}V_{0.1}Fe_{0.5}Ni_{0.5}$ (figure 3(a)) is due to the formation of Mg–Ti solid solution. The composite nature of the alloy particles with Mg matrix is confirmed from the microstructural studies of these composite materials using scanning electron microscopy (SEM). SEM and EDAX of Mg + x wt% $Ti_{0.1}Zr_{0.9}Mn_{0.9}V_{0.1}Fe_{0.5}Ni_{0.5}$ (x = 25, 40, 50 and 75) composites confirm that the smaller bright phases correspond to $Ti_{0.1}Zr_{0.9}Mn_{0.9}V_{0.1}Fe_{0.5}Ni_{0.5}$ particles and the dark background phase corresponds to Mg matrix (figure 4).

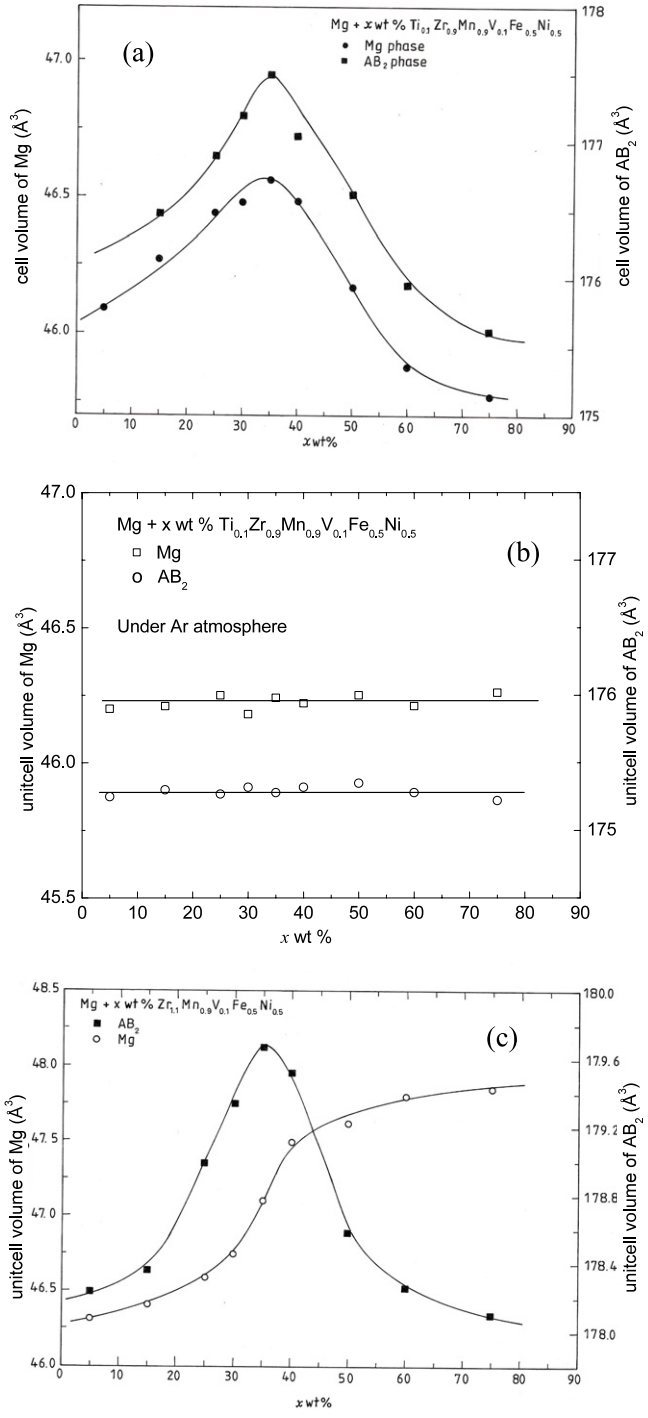

Figure 3. Variation of unit cell volumes of Mg and AB_2 alloy phase with the amount of catalyst (x) in Mg+x wt% $Ti_{0.1}Zr_{0.9}Mn_{0.9}V_{0.1}Fe_{0.5}Ni_{0.5}$ (x = 5, 15, 25, 30, 35, 40, 50, 60 and 75) (a) prepared under H_2 atmosphere, (b) prepared under Ar atmosphere and (c) Mg+x wt% $ZrMn_{0.9}V_{0.1}Fe_{0.5}Ni_{0.5}$ (x = 5, 15, 25, 30, 35, 40, 50, 60 and 75) prepared under H_2 atmosphere.

Table 1. Lattice parameters and unit cell volumes of Mg and AB_2 phases in Mg + x wt% $Ti_{0.1}Zr_{0.9}Mn_{0.9}V_{0.1}Fe_{0.5}Ni_{0.5}$ (x = 5, 15, 25, 30, 35, 40, 50, 60 and 75) composite materials. (The values of a and c have an accuracy of 0.001 Å. The values of the unit cell volume are given with an accuracy 0.02 (Å^3).)

	AB_2 phase			Mg phase		
Material	a (Å)	c (Å)	v (Å^3)	a (Å)	c (Å)	v (Å^3)
Mg + 5 wt% $Ti_{0.1}Zr_{0.9}Mn_{0.9}V_{0.1}Fe_{0.5}Ni_{0.5}$	—	—	—	3.202	5.195	46.09
Mg + 15 wt% $Ti_{0.1}Zr_{0.9}Mn_{0.9}V_{0.1}Fe_{0.5}Ni_{0.5}$	4.999	8.155	176.48	3.206	5.199	46.27
Mg + 25 wt% $Ti_{0.1}Zr_{0.9}Mn_{0.9}V_{0.1}Fe_{0.5}Ni_{0.5}$	5.001	8.168	176.90	3.212	5.199	46.44
Mg + 30 wt% $Ti_{0.1}Zr_{0.9}Mn_{0.9}V_{0.1}Fe_{0.5}Ni_{0.5}$	5.005	8.169	177.20	3.213	5.202	46.48
Mg + 35 wt% $Ti_{0.1}Zr_{0.9}Mn_{0.9}V_{0.1}Fe_{0.5}Ni_{0.5}$	5.008	8.172	177.50	3.214	5.204	46.56
Mg + 40 wt% $Ti_{0.1}Zr_{0.9}Mn_{0.9}V_{0.1}Fe_{0.5}Ni_{0.5}$	5.003	8.166	177.00	3.212	5.202	46.48
Mg + 50 wt% $Ti_{0.1}Zr_{0.9}Mn_{0.9}V_{0.1}Fe_{0.5}Ni_{0.5}$	5.000	8.158	176.62	3.198	5.194	46.05
Mg + 60 wt% $Ti_{0.1}Zr_{0.9}Mn_{0.9}V_{0.1}Fe_{0.5}Ni_{0.5}$	4.990	8.160	175.95	3.191	5.202	45.88
Mg + 75 wt% $Ti_{0.1}Zr_{0.9}Mn_{0.9}V_{0.1}Fe_{0.5}Ni_{0.5}$	4.992	8.138	175.62	3.190	5.194	45.77

Table 2. Plateau pressure, hydrogen storage capacity, plateau slope and rate constants in [Mg + x wt% $Ti_{0.1}Zr_{0.9}Mn_{0.9}V_{0.1}Fe_{0.5}Ni_{0.5}$]–H ($x$ = 5, 15, 25, 30, 35, 40, 50, 60 and 75).

Hydride	Plateau pressure[a] (bar)	Storage capacity (wt%)	Plateau slope	k ($\alpha + \beta$) phase (s^{-1})	k β phase (s^{-1})
[Mg + 5 wt% $Ti_{0.1}Zr_{0.9}Mn_{0.9}V_{0.1}Fe_{0.5}Ni_{0.5}$]–H	3.5	4.8	1.6	5.38×10^{-3} [b]	3.74×10^{-4} [b]
[Mg + 15 wt% $Ti_{0.1}Zr_{0.9}Mn_{0.9}V_{0.1}Fe_{0.5}Ni_{0.5}$]–H	2.1	4.1	1.4	8.11×10^{-3} [b]	5.10×10^{-4} [b]
[Mg + 25 wt% $Ti_{0.1}Zr_{0.9}Mn_{0.9}V_{0.1}Fe_{0.5}Ni_{0.5}$]–H	1.6	3.4	1.5	1.24×10^{-2}	9.49×10^{-4}
[Mg + 30 wt% $Ti_{0.1}Zr_{0.9}Mn_{0.9}V_{0.1}Fe_{0.5}Ni_{0.5}$]–H	0.8	3.3	1.1	1.45×10^{-2}	1.10×10^{-3}
[Mg + 35 wt% $Ti_{0.1}Zr_{0.9}Mn_{0.9}V_{0.1}Fe_{0.5}Ni_{0.5}$]–H	0.65	3.2	1.0	1.62×10^{-2}	1.25×10^{-3}
[Mg + 40 wt% $Ti_{0.1}Zr_{0.9}Mn_{0.9}V_{0.1}Fe_{0.5}Ni_{0.5}$]–H	1.1	3.1	0.6	1.97×10^{-2}	1.49×10^{-3}
[Mg + 50 wt% $Ti_{0.1}Zr_{0.9}Mn_{0.9}V_{0.1}Fe_{0.5}Ni_{0.5}$]–H	2.0	2.2	0.5	2.85×10^{-2}	1.97×10^{-3}
[Mg + 60 wt% $Ti_{0.1}Zr_{0.9}Mn_{0.9}V_{0.1}Fe_{0.5}Ni_{0.5}$]–H	4.8	1.9	1.1	3.56×10^{-2}	2.95×10^{-3}
[Mg + 75 wt% $Ti_{0.1}Zr_{0.9}Mn_{0.9}V_{0.1}Fe_{0.5}Ni_{0.5}$]–H	18.5	1.8	1.6	4.85×10^{-2}	5.56×10^{-3}

[a] The plateau pressure is measured at the mid-point of the plateau region.
[b] Values obtained from second-order fitting.

3.2. P–C isotherms

Hydrogen absorption isotherms of Mg + x wt% $Ti_{0.1}Zr_{0.9}Mn_{0.9}V_{0.1}Fe_{0.5}Ni_{0.5}$ (x = 5, 15, 25, 30, 35, 40, 50, 60 and 75) composite materials have been studied in the pressure range 0.1–30 bar and at 300 °C using the pressure reduction technique and are shown in figure 5. The P–C isotherms show that there are two single-phase regions (α and β) and one plateau region ($\alpha + \beta$) present in these systems within the pressure ranges studied. The storage capacity and the plateau pressure ($P_{\alpha\to\beta}$) of the composite material depend on the number of catalytic alloy particles. $P_{\alpha\to\beta}$ is measured at the mid-point of the plateau region. For technical applications plateau slope can be represented as plateau slope factor, which is given by $\ln(P_1/P_2)$, where P_1 represents the $\alpha \to (\alpha + \beta)$ phase transition pressure and P_2 represents the $(\alpha + \beta) \to \beta$ phase transition pressure, where there is a change in slope [18]. The distance between P_1 and P_2 is the plateau width and the pressure at the mid-point of the plateau width is called the plateau pressure. Table 2 gives $P_{\alpha\to\beta}$, hydrogen storage capacity and the plateau slope of [Mg + x wt% $Ti_{0.1}Zr_{0.9}Mn_{0.9}V_{0.1}Fe_{0.5}Ni_{0.5}$]–H ($x$ = 5, 15, 25, 30, 35, 40, 50, 60 and 75). $P_{\alpha\to\beta}$ decreases as x increases up to 35 wt% and then there is an increase (figure 6). The

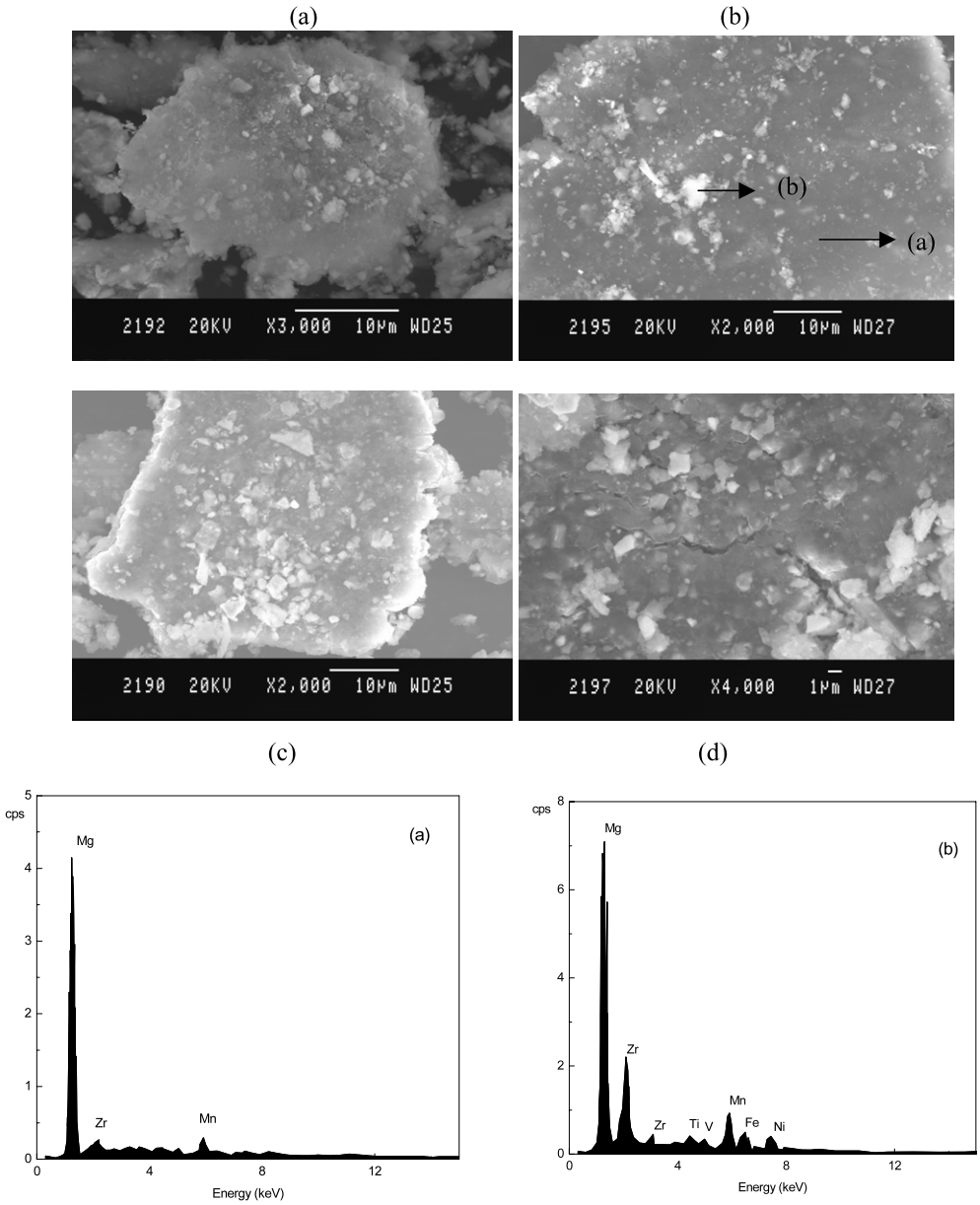

Figure 4. SEM image and EDAX patterns of Mg+x wt% $Ti_{0.1}Zr_{0.9}Mn_{0.9}V_{0.1}Fe_{0.5}Ni_{0.5}$ composite material: (a) $x = 25$, (b) $x = 40$, (c) $x = 50$, (d) $x = 75$.

unit cell volumes of Mg and alloy phases increase up to $x = 35$ wt% (table 1 and figure 3), which causes an decrease in strain energy to accommodate the interstitial hydrogen; this results in the decrease of $P_{\alpha\rightarrow\beta}$ with increase of x up to about 35 wt%. For $x > 35$ wt%, the unit cell volumes of both phases decrease, thereby increasing $P_{\alpha\rightarrow\beta}$. From the P–C isotherms it is found that the hydrogen storage capacity of these composites decreases with increase of alloy content, which is due to low storage capacity of catalytic AB_2 alloy. Even though the increase of

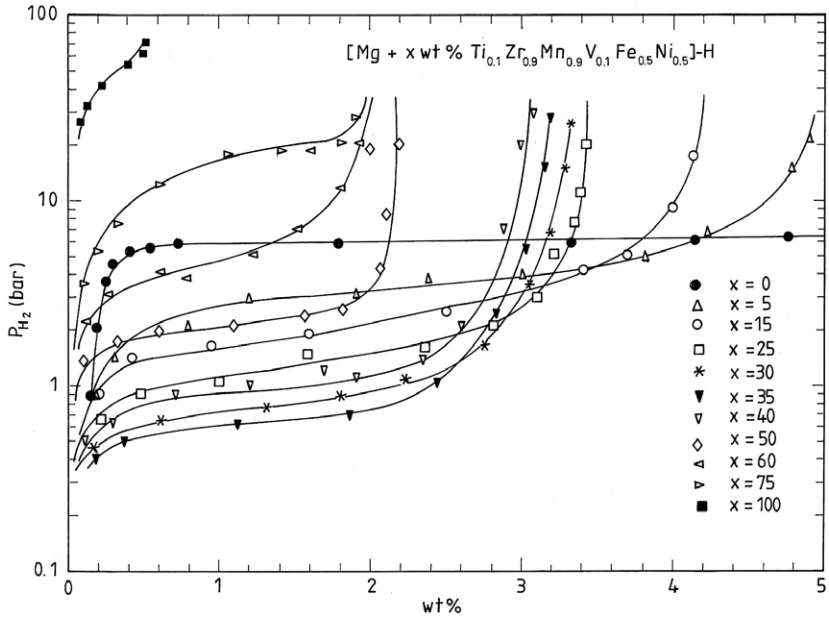

Figure 5. Pressure–composition isotherms of Mg + x wt % $Ti_{0.1}Zr_{0.9}Mn_{0.9}V_{0.1}Fe_{0.5}Ni_{0.5}$ (x = 5, 15, 25, 30, 35, 40, 50, 60 and 75) composite materials at 300 °C.

catalyst results in lower storage capacity, it is observed that the reaction between hydrogen and composite material is fast for higher catalyst composite material. Maximum storage capacity is found to be 4.8 wt% in Mg + 5 wt% $Ti_{0.1}Zr_{0.9}Mn_{0.9}V_{0.1}Fe_{0.5}Ni_{0.5}$ at 300 °C.

Figure 7 shows the pressure–composition absorption/desorption isotherms of Mg + 25 wt% $Ti_{0.1}Zr_{0.9}Mn_{0.9}V_{0.1}Fe_{0.5}Ni_{0.5}$ composite material in the temperature range 200–350 °C. A single plateau region is observed in the pressure and temperature ranges studied and the hydrogen concentration increases with decreasing temperature. Energy loss per cycle of absorption and desorption can be obtained from the pressure difference between the absorption and desorption isotherms using $\Delta G_{\text{loss}} = \frac{1}{2}RT\ln(\frac{P_a}{P_d})$, where P_a (1.6 bar) and P_d (0.7 bar) are the absorption and desorption plateau pressure respectively, and the value is 1.99 kJ mol^{-1} H at 300 °C.

3.3. Thermal desorption behaviour

Figure 8 shows the DSC curves of Mg + x wt% $Ti_{0.1}Zr_{0.9}Mn_{0.9}V_{0.1}Fe_{0.5}Ni_{0.5}$–H ($x$ = 5, 15, 40, 50, 60 and 75) composite materials with maximum hydrogen concentration under Ar atmosphere with heat rate 10 °C min^{-1} in the temperature range 200–550 °C. DSC curves show a double endothermic peak, which is due to the hydrogen desorption from the composite hydride. For x = 5 wt% composite, the desorption peak temperatures are 448 and 491 °C. Further, the desorption peaks shift towards lower temperature as the number of alloy particles increases, which is due to the more dispersed alloy particles acting as a diffusion path for hydrogen. Previous thermal studies of MgH_2 show an endothermic peak around 450 °C associated with the hydrogen desorption from β-MgH_2 [19–21]. The double endothermic peak observed in the present work shows that two processes with different kinetics are occurring. Gennari *et al* reported that the mechanically milled MgH_2 shows double endothermic peaks correspond to the hydrogen desorption from β-MgH_2 and γ-MgH_2 [22].

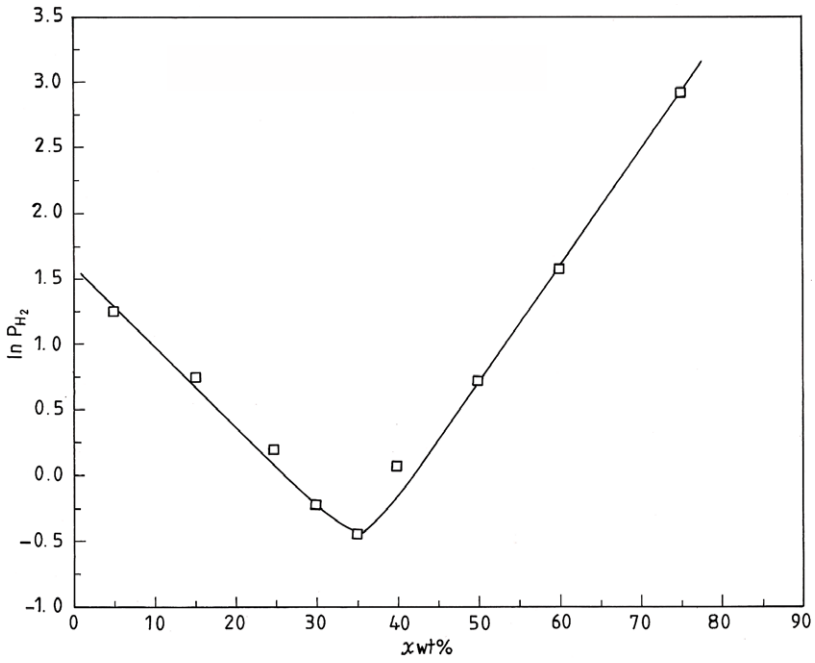

Figure 6. Dependence of plateau pressure on the amount of catalyst (x) in [Mg + x wt% $Ti_{0.1}Zr_{0.9}Mn_{0.9}V_{0.1}Fe_{0.5}Ni_{0.5}$]–H.

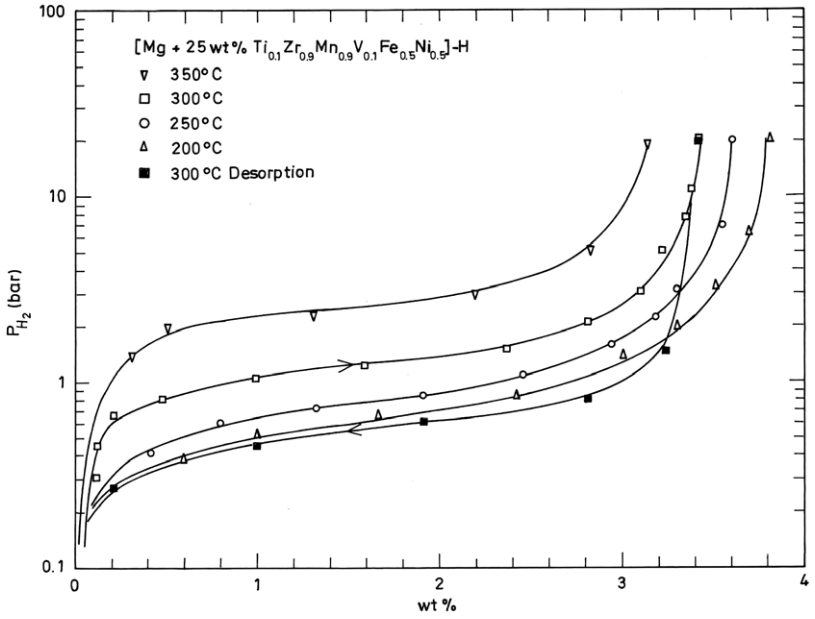

Figure 7. P–C absorption/desorption isotherms of Mg + 25 wt% $Ti_{0.1}Zr_{0.9}Mn_{0.9}V_{0.1}Fe_{0.5}Ni_{0.5}$ composite material at different temperatures.

Further, our previous thermal desorption studies of AB_2 alloy hydrides show that the hydrogen desorption temperature is around 220 °C [13]. Hence, the high-temperature peak is due to the

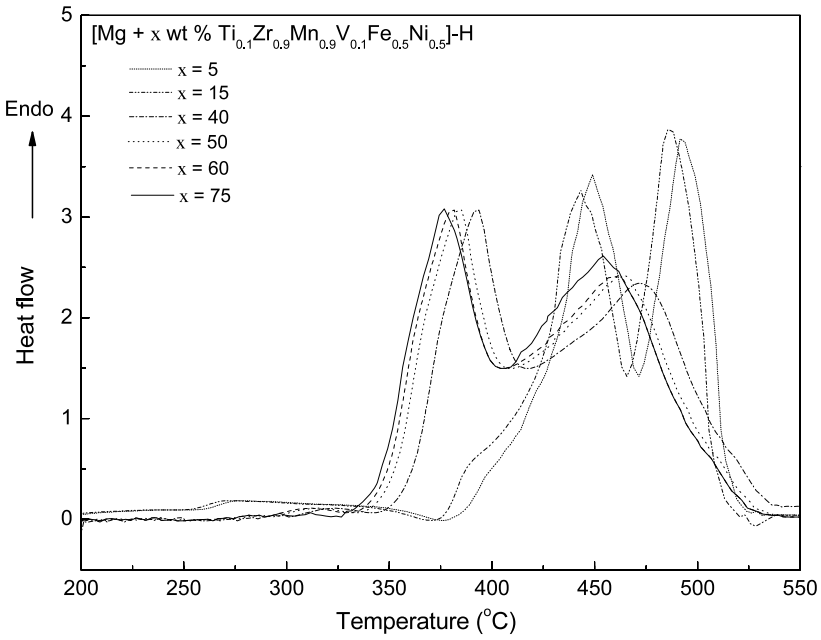

Figure 8. DSC curves of Mg + x wt% $Ti_{0.1}Zr_{0.9}Mn_{0.9}V_{0.1}Fe_{0.5}Ni_{0.5}$ (x = 5, 15, 40, 50, 60 and 75) composites.

hydrogen desorption from β-MgH_2 and the low-temperature peak is associated with hydrogen desorption from both γ-MgH_2 and β-MgH_2.

3.4. Analysis of reaction kinetics

The hydrogen absorption/desorption kinetics measurements in Mg+x wt% $Ti_{0.1}Zr_{0.9}Mn_{0.9}V_{0.1}Fe_{0.5}Ni_{0.5}$ (x = 5, 15, 25, 30, 35, 40, 50, 60 and 75) composites were performed at 300 °C and those in Mg + 25 wt% $Ti_{0.1}Zr_{0.9}Mn_{0.9}V_{0.1}Fe_{0.5}Ni_{0.5}$ were performed in the temperature range 250–325 °C by measuring the pressure change during the hydrogen absorption/desorption process (figures 9 and 10). It can be seen that the rate of hydrogen absorption/desorption is much faster than the rate of hydrogen desorption. For example, for x = 75 wt% composite, the absorption of hydrogen is nearly complete in 2 min (figure 9(a)), while the desorption reaches completion in 30 min (figure 9(b)). The kinetics data show that the rate of absorption is fast for the composite material with higher x, which is due to the dispersion of $Ti_{0.1}Zr_{0.9}Mn_{0.9}V_{0.1}Fe_{0.5}Ni_{0.5}$ alloy particles on the surface of the Mg matrix and dissociation of hydrogen molecules into atoms more easily due to catalytic alloy particles. In alloy hydrides, when the reactions proceed through different phase regions, the absorption rate will be controlled by different mechanisms. The surface process, the interface process and diffusion are the possible rate determining steps involved in the hydrogen absorption kinetics. The surface process, chemisorption and nucleation of the hydrides occur at the initial stage of absorption. As the absorption process proceeds further, the hydride phase nuclei start growing. After some time, the growing hydride phase nuclei contact with each other with a corresponding decrease in interfacial area and in this process the reaction rate is controlled by the phase transformation at the $\alpha \rightarrow \beta$ interface. When the β phase hydride is formed completely, the diffusion of hydrogen should constitute the rate-determining step [23, 24]. Therefore, there

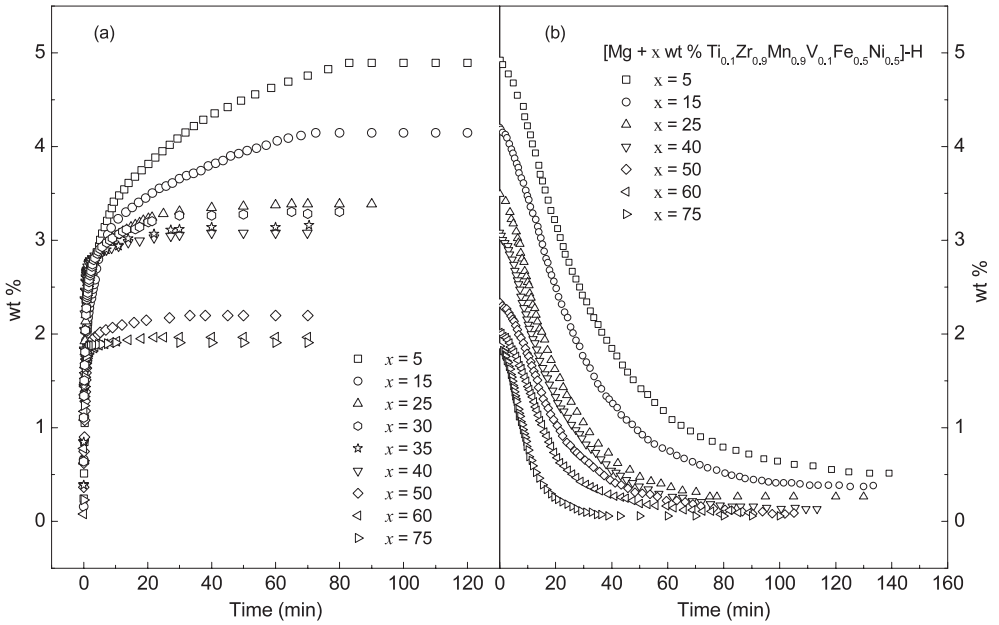

Figure 9. Kinetics of hydrogen absorption/desorption of Mg+x wt% $Ti_{0.1}Zr_{0.9}Mn_{0.9}V_{0.1}Fe_{0.5}Ni_{0.5}$ (x = 5, 15, 25, 30, 35, 40, 50, 60 and 75) composite materials at 300 °C.

are three different reaction mechanisms corresponding to the three phase regions involved. In the present investigation of hydrogen absorption of Mg + x wt% $Ti_{0.1}Zr_{0.9}Mn_{0.9}V_{0.1}Fe_{0.5}Ni_{0.5}$ (x = 5, 15, 25, 30, 35, 40, 50, 60 and 75) the hydrogen reaction mechanism is analysed using the Avrami–Erofeev rate equation

$$F = 1 - e^{-kt^n} \tag{1}$$

where F is the fractional hydrogen concentration, k is the reaction rate constant and n is the reaction order. The reaction order (n) is found by fitting the experimental data with different rate equations. When the order is assumed, the rate equation which best fits the observed data can be found for the appropriate value of the order (n). For x = 25, 30, 35, 40, 50, 60 and 75 composites, the reaction order was determined as 1.0 for all phases by fitting the experimental data. Hence the rate equation becomes (first-order rate equation) $-\ln(1-F) = kt$. For x = 5 and 15; the experimental data fit into the second-order rate equation $[-\ln(1-F)]^{1/2} = kt$. Figures 11(a) and (b) show the first- and second-order fitting of the experimental data for Mg+x wt% $Ti_{0.1}Zr_{0.9}Mn_{0.9}V_{0.1}Fe_{0.5}Ni_{0.5}$ (x = 5, 15, 25, 30, 35, 40, 50, 60 and 75) composites measured at 300 °C. It may be seen from figure 11 that the experimental data fit to two linear segments and a gradual slope change occurs.

Kinetics of hydrogen absorption of Mg+25 wt% $Ti_{0.1}Zr_{0.9}Mn_{0.9}V_{0.1}Fe_{0.5}Ni_{0.5}$ at different temperatures have been analysed using a first-order rate equation and the results are shown in figure 12. It was found from the P–C isotherms that the concentration at which the slope changes corresponds to the $\alpha + \beta$ phase to β phase transition region [25]. The first linear segment corresponds to the ($\alpha + \beta$) phase and the second one to the β phase and the rate constants have been obtained from the slope of the fitting. The surface process, chemisorption and nucleation of the hydrides occur at the initial stage of absorption, which seem to be unnoticed in our case, because of the fast reaction kinetics in the α phase. The values of rate constant in the $\alpha + \beta$ phase and β phase for [Mg + x wt% $Ti_{0.1}Zr_{0.9}Mn_{0.9}V_{0.1}Fe_{0.5}Ni_{0.5}$]–H

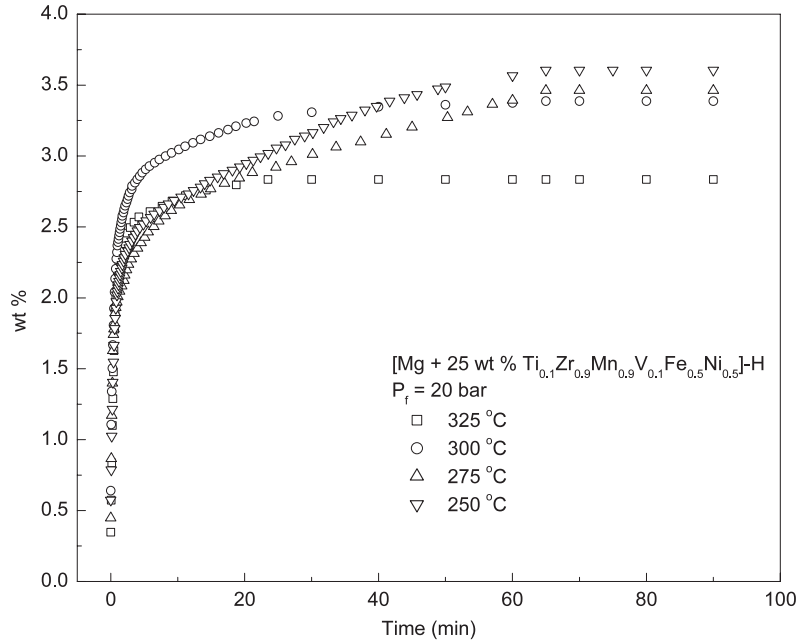

Figure 10. Kinetics of hydrogen absorption of Mg + 25 wt% $Ti_{0.1}Zr_{0.9}Mn_{0.9}V_{0.1}Fe_{0.5}Ni_{0.5}$ composite material at different temperatures.

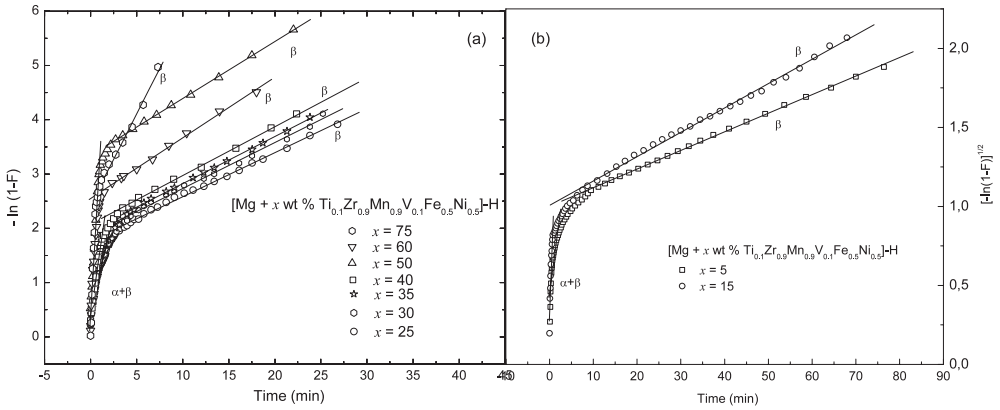

Figure 11. (a) $-\ln(1-F)$ versus t plots of [Mg + x wt% $Ti_{0.1}Zr_{0.9}Mn_{0.9}V_{0.1}Fe_{0.5}Ni_{0.5}$]–H ($x$ = 25, 30, 35, 40, 50, 60 and 75). (b) $[-\ln(1-F)]^{1/2}$ versus t plots of [Mg + x wt% $Ti_{0.1}Zr_{0.9}Mn_{0.9}V_{0.1}Fe_{0.5}Ni_{0.5}$]–H ($x$ = 5 and 15).

(x = 5, 15, 25, 30, 35, 40, 50, 60 and 75) are listed in table 2. The variation of rate constant in the $\alpha + \beta$ phase and β phase with the amount of catalyst (figure 13(a)) shows that the reaction kinetics exponentially increases with the amount of catalyst. The hydrogen absorption reaction mechanism in these composites can be explained using (1) dispersion of alloy particles over the Mg matrix, as seen from the SEM images (figure 4), which can dissociate hydrogen molecules more easily and will provide a path for hydrogen diffusion through the Mg matrix, and (2) the exothermic nature of hydrogen absorption by these AB_2 alloys will release a large amount of heat; this thermal energy can be utilized to improve the kinetics of hydrogen absorption by

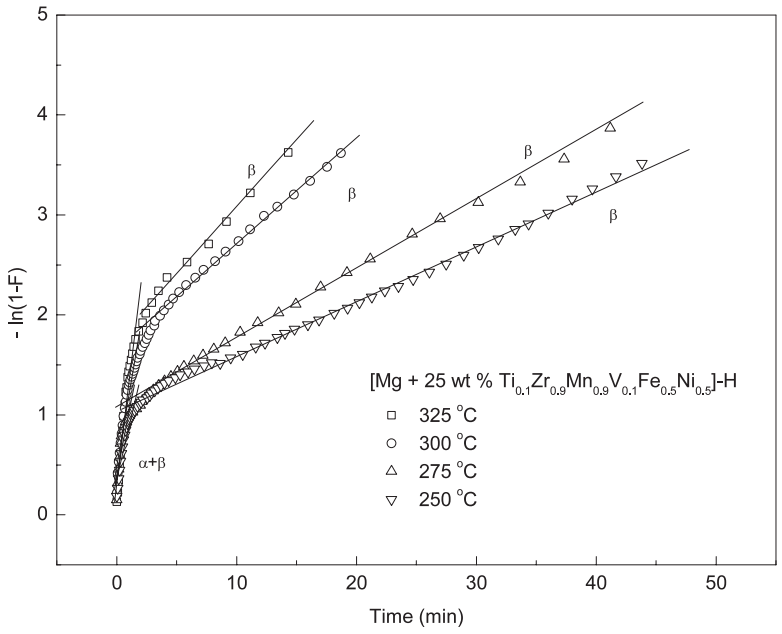

Figure 12. $-\ln(1-F)$ versus t plots of [Mg + 25 wt% $Ti_{0.1}Zr_{0.9}Mn_{0.9}V_{0.1}Fe_{0.5}Ni_{0.5}$]–H at different temperatures.

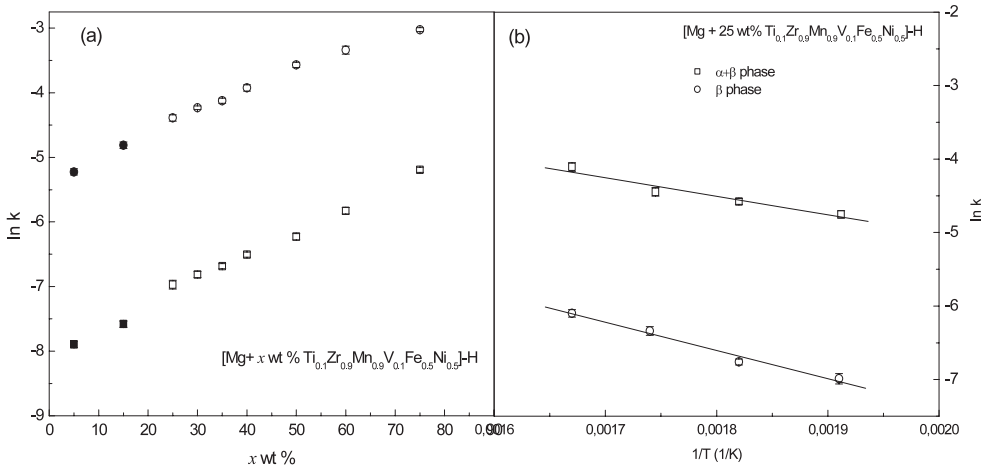

Figure 13. (a) Dependence of $\ln k$ on the amount of catalyst (x) in [Mg + x wt% $Ti_{0.1}Zr_{0.9}Mn_{0.9}V_{0.1}Fe_{0.5}Ni_{0.5}$]–H ($x$ = 5, 15, 25, 30, 35, 40, 50, 60 and 75) (first order, ○ $\alpha+\beta$ phase and □ β phase; second order, ● $\alpha+\beta$ phase and ■ β phase). (b) $\ln k$ versus $1/T$ plot for $\alpha+\beta$ phase and β phase for [Mg + 25 wt% $Ti_{0.1}Zr_{0.9}Mn_{0.9}V_{0.1}Fe_{0.5}Ni_{0.5}$]–H.

these composites. The main hydride phase in these composites is Mg powder and the AB_2 alloy only absorbs a small amount (>0.5 wt% at 300 °C) of hydrogen. The variation of rate constant with temperature in $(\alpha+\beta)$ phase and β phase for Mg + 25 wt% $Ti_{0.1}Zr_{0.9}Mn_{0.9}V_{0.1}Fe_{0.5}Ni_{0.5}$ obeys the Arrhenius relation (figure 13(b)). The values of activation energy in the $\alpha+\beta$ phase and β phase have been obtained from the slope of the Arrhenius plot and are 220 ± 6

and 332 ± 8 meV in the $\alpha + \beta$ phase and β phase respectively. Hydrogen storage properties of Mg composites reveal that the composites with 5 and 15 wt% alloy content have good hydrogen storage capacity. However, the $x = 15$ wt% composite has faster kinetics than the $x = 5$ wt % composite and the storage capacity of the latter is high. The composites with $x = 25$, 30, 35 and 40 wt% alloy content form stable hydrides. Further, $x = 50$, 60 and 75 wt% composites have fast absorption/desorption kinetics. However, the low storage capacity of these composites limits their applications. Hence, $x = 5$ wt% composite seems to be a most favourable material, with hydrogen storage capacity of 4.8 wt% and reasonable kinetics of hydrogen absorption. Previous hydrogen storage properties of Mg–$ZrCr_2$ composites show a maximum hydrogen storage capacity of 1.5 wt% at 530 K [26]. Hydriding/dehydriding properties of mechanically milled Mg–30 wt% $TiMn_{1.5}$ composite material reveal a maximum storage capacity of 4.4 wt% at 573 K [10]. In the present investigation a maximum storage capacity of around 4.8 wt% is obtained in Mg + 5 wt% $Ti_{0.1}Zr_{0.9}Mn_{0.9}V_{0.1}Fe_{0.5}Ni_{0.5}$.

4. Conclusion

X-ray diffraction studies of these composites reveal that the unit cell volumes of Mg and AB_2 phases decrease after $x = 40$ wt% due to the formation of Mg–Ti solid solution and Mg_6Ni secondary phase. Hydrogen absorption isotherms of Mg + x wt% $Ti_{0.1}Zr_{0.9}Mn_{0.9}V_{0.1}Fe_{0.5}Ni_{0.5}$ ($x = 5$, 15, 25, 30, 35, 40, 50, 60 and 75) composites show the presence of a single plateau region. Hydrogen storage capacity increases with decrease of $Ti_{0.1}Zr_{0.9}Mn_{0.9}V_{0.1}Fe_{0.5}Ni_{0.5}$, and a maximum storage capacity of around 4.8 wt% is obtained in Mg + 5 wt% $Ti_{0.1}Zr_{0.9}Mn_{0.9}V_{0.1}Fe_{0.5}Ni_{0.5}$. Since the dispersed alloy particles provide a path for hydrogen diffusion through the Mg matrix, the kinetics of hydrogen absorption is faster in Mg + 75 wt% $Ti_{0.1}Zr_{0.9}Mn_{0.9}V_{0.1}Fe_{0.5}Ni_{0.5}$. The hydrogen absorption rate constants in the $(\alpha + \beta)$ and β phases of [Mg + x wt% $Ti_{0.1}Zr_{0.9}Mn_{0.9}V_{0.1}Fe_{0.5}Ni_{0.5}$]–H ($x = 5$, 15, 25, 30, 35, 40, 50, 60 and 75) are in the ranges 5.4×10^{-3}–4.8×10^{-2} s^{-1} and 3.7×10^{-4}–5.6×10^{-3} s^{-1} respectively. The activation energies obtained from the kinetics of hydrogen absorption measurements of Mg + 25 wt% $Ti_{0.1}Zr_{0.9}Mn_{0.9}V_{0.1}Fe_{0.5}Ni_{0.5}$ at different temperatures are 220 ± 6 and 332 ± 8 meV in the $(\alpha + \beta)$ phase and β phase respectively.

Acknowledgments

The authors are grateful to DRDO and MNES, Government of India, for supporting this work. One of the authors (MK) is grateful to IITM, Chennai, for financial support.

References

[1] Bogdanovic B, Bohmhammel K, Chris B, Reiser A, Schlichte K, Vehlen R and Wolf U 1999 *J. Alloys Compounds* **282** 84
[2] Yang J, Ciureanu M and Roderge R 2000 *Mater. Lett.* **43** 234
[3] Zaluska A, Zaluski L and Strom-Olsen J O 2001 *Appl. Phys.* A **72** 157
[4] Barkhordarian G, Klassen T and Bormann R 2003 *Scr. Mater.* **49** 213
[5] Huot J, Liang G and Schulz R 2001 *Appl. Phys.* A **72** 187
[6] Bobet J L, Castro F J and Chevalier B 2005 *Scr. Mater.* **52** 33
[7] Wang P, Zhang H F, Ding B Z and Hu Z Q 2001 *Acta Mater.* **49** 921
[8] Sun D, Gingl F, Enoki H, Ross D K and Akiba E 2000 *Acta Mater.* **48** 2363
[9] Zaluska A, Zaluski L and Strom-Olsen J O 1999 *J. Alloys Compounds* **288** 217
[10] Hu Y Q, Zhang H F, Wang A M, Ding B Z and Hu Z Q 2003 *J. Alloys Compounds* **354** 296
[11] Kandavel M and Ramaprabhu S 2003 *J. Phys.: Condens. Matter* **15** 7501–17

[12] Kiyobayashi T, Takeshita H T, Tanaka H, Takeichi N, Zuttel A, Schlapbach L and Kuriyama N 2002 *J. Alloys Compounds* **330–332** 666
[13] Kandavel M and Ramaprabhu S 2006 *J. Phys.: Condens. Matter* **18** 2943–54
[14] Schimmel H G, Hout J, Chapon L C, Tichelaar F D and Mulder F M 2005 *J. Am. Chem. Soc.* **127** 14348
[15] Roberts C S 1960 *Magnesium and its Alloys* (New York: Wiley)
[16] Liang G and Schulz R 2003 *J. Mater. Sci.* **38** 1179
[17] Liang G and Schulz R 2002 *J. Metastable Nanocryst. Mater.* **12** 93
[18] Kandavel M and Ramaprabhu S 2004 *J. Alloys Compounds* **381** 140
[19] Huot J, Akiba E and Takada T 1995 *J. Alloys Compounds* **231** 815
[20] Zaluska A, Zaluski L and Strom-Olsen J O 1999 *J. Alloys Compounds* **289** 197
[21] Shang C X and Guo Z X 2004 *J. Power Sources* **129** 73–80
[22] Gennari F C, Castro F J and Urretavizcaya G 2001 *J. Alloys Compounds* **321** 46–53
[23] Ramesh R and Rama Rao K V S 1993 *J. Alloys Compounds* **191** 101
[24] Koh J T, Goudy A J, Huang P and Zhou G 1989 *J. Less-Common Met.* **153** 89
[25] Sivakumar R, Ramaprabhu S, Rama Rao K V S, Anton H and Schmidt P C 2000 *Int. J. Hydrog. Energy* **25** 463
[26] Farnandez J F, Bodega J and Sanchez C R 2003 *J. Alloys Compounds* **356/357** 343

J. Phys.: Condens. Matter **20** (2008) 179801 (2pp) doi:10.1088/0953-8984/20/17/179801

Erratum

Hydrogen storage properties of Mg-based composites prepared by reaction ball milling
M Kandavel and S Ramaprabhu *J. Phys.: Condens. Matter* **18** 11275–11290

Figure 3(c) and figure 4 given in the above paper for Mg + stoichiometric Zr-based AB_2 [Mg + x wt% $Ti_{0.1}Zr_{0.9}Mn_{0.9}V_{0.1}Fe_{0.5}Ni_{0.5}$ (x = 5, 15, 25, 30, 35, 40, 50, 60 and 75)] composites are incorrect. These two figures are for Mg + non-stoichiometric Zr-based AB_2 [Mg + x wt% $(Ti_{0.1}Zr_{0.9})_{1.1}Mn_{0.9}V_{0.1}Fe_{0.5}Ni_{0.5}$ (x = 5, 15, 25, 30, 35, 40, 50, 60 and 75)] composites. The results for Mg + non-stoichiometric Zr-based AB_2 composites have been published in *J. Alloys Compounds* **438** 285–92 in the research paper titled 'Correlation between hydrogen storage properties and amount of alloy particles in Mg-based composites'. Figure 3(c) and figure 4 given in *J. Phys.: Condens. Matter* **18** 11275–90 should be replaced by the following two figures. These mistakes are entirely the fault of the authors and the authors regret these errors.

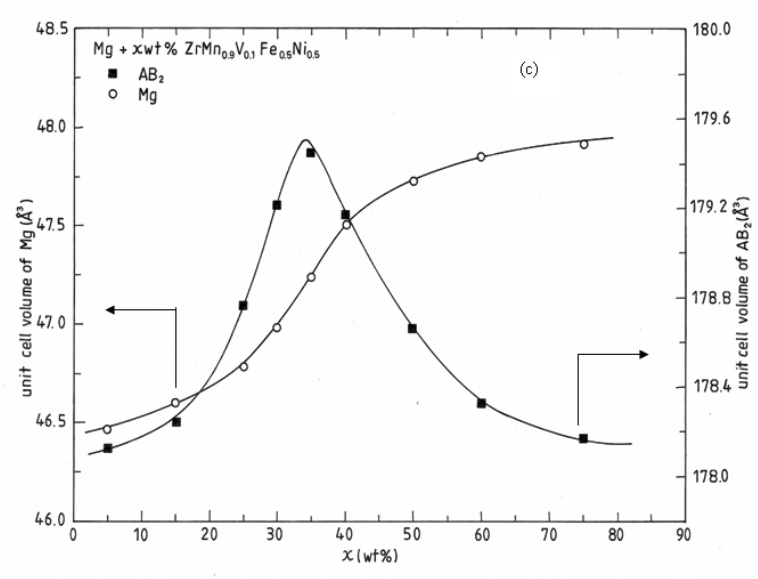

Figure 3 (c). Variation of unit cell volume of Mg and AB_2 alloy phase with the amount of catalyst (x) in Mg + x wt% $Ti_{0.1}Zr_{0.9}Mn_{0.9}V_{0.1}Fe_{0.5}Ni_{0.5}$ (x = 5, 15, 25, 30, 35, 40, 50, 60 and 75) prepared under H_2 atmosphere.

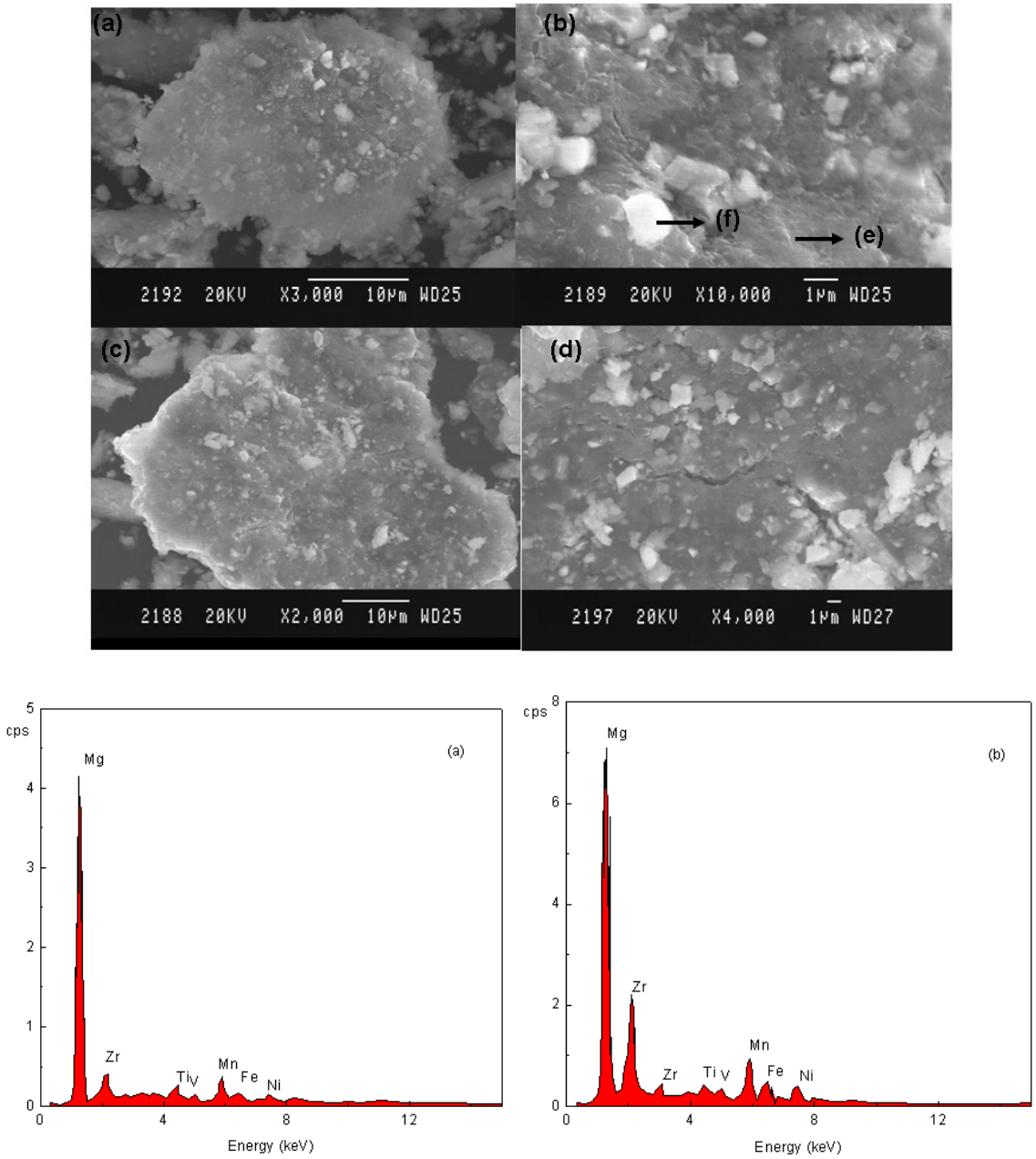

Figure 4. SEM image and EDAX patterns of Mg + x wt% $Ti_{0.1}Zr_{0.9}Mn_{0.9}V_{0.1}Fe_{0.5}Ni_{0.5}$ composite material: (a) $x = 25$, (b) $x = 40$, (c) $x = 50$, (d) $x = 75$.